Modeling and Implementation of a Long-Distance Seawater Single-Wire CPT System for Underwater Sensor

Chenghao Li, *Student Member, IEEE*, Xiuyun Ren, *Member, IEEE*, Xichen Liu, *Student Member, IEEE*, Shuai Wu, *Member, IEEE*, Mingdong Qi, Jinpeng Yu, *Senior Member, IEEE*, and Chunwei Cai, *Member, IEEE*

***Abstract*—A long-distance, strong-misalignment tolerance seawater capacitive power transfer system with two insulated electric-field couplers and single-wire for underwater sensors is proposed in this article, and it has the advantages of low cost, low weight and hard worn-out compared with traditional structure. First, quasi electric double layer theory for coupler in seawater is proposed, and seawater between two couplers can be considered as equipotential medium is demonstrated in detail. Second, model of seawater electric-field coupled channel is built. The feasibility of long distance and strong misalignment tolerance is proved. Then, double *T-LCL* compensation network is investigated and selected for constant output voltage, zero phase angle (ZPA), and antifrequency-offset. Experimental results in lab show that the system can deliver 732.1 W at a dc–dc efficiency of 89.2%. In actual ocean, the experimental transmission distance is 10 m, achieving 206.8 W power transmission and 83% efficiency, which verifies the proposed program is adapted to power supply of sensors in complex ocean environment and the advantages of long distance. This article is also accompanied by a video file demonstrating experiment in actual ocean.**

***Index Terms*—Quasi electric double layer (Q-EDL), seawater capacitive power transfer(SCPT), single-wire, undersea sensors.**

I. Introduction

NOWDAYS, ocean monitoring has obtained a broad attention, as it enables to monitor marine environment, including temperature, salinity, seismicity, geomagnetic variation, and currents over long periods, offering ocean data in real-time [1]. Underwater sensor is playing an essential role in ocean monitoring, attracting great interests [2]. However, the battery of the underwater sensor needs to be replaced frequently when it runs low on power, which is costly and not suitable for long measurement period. Therefore, the realization of real-time power supply will dramatically enhance the performance of ocean monitoring [3].

At present, there is one program that a mooring cable is utilized to transfer power from buoys to underwater sensors in long distance [4], [5], [6], which forms a closed power circuit. The buoy on surface provides energy, and mooring cable connects buoy and sensors, serving as the power link with a relatively fixed structure [4], [5]. Cai et al. [6] proposes three typical mooring structures with different geometries, expanding the application scenarios furtherly. Nevertheless, mooring cable of these papers is made up of two strands of conductor wire twisted together at least to form a closed power circuit, leading to high cost, high weight and easy worn-out.

Wireless power transfer (WPT) has been extensively studied because of convenience and safety [7], [8]. Based on inductive power transfer (IPT), researchers have proposed various technologies for undersea sensors [9], [10], [11], [12], [13]. Sensor nodes derive power from mooring cables via magnetic coupling devices, while the mooring cable is both the upper coupler's secondary winding and the lower coupler's primary winding [9], [10]. For a more refined analysis, Maxwell equations are established and analyzed to conclude that the electromagnetic wave is bound to propagate on the surface of the mooring cable [11]. Furthermore, double ultracapacitor chargers using indirect control [12] and maximum efficiency tracking [13] are investigated, enriching the application scenarios. However, all these programs exist the problem that couplers are mounted on the mooring cables directly, causing inevitable sliding wear. Besides, IPT also has the defects of high eddy loss in metallic shell, limited distance and misalignment tolerance with the complex marine environment.

Capacitive power transfer (CPT) has numerous advantages, including reduced size, light weight, lower eddy current loss compared with IPT [14] and has the potential in marine equipment [15], [16], [17], [18], [19], [20], [21], [22], [23], [24], [25], [26]. If the medium is divided into pure water, freshwater and seawater, it can be found that due to the high conductivity 4 S/m

Received 18 November 2024; revised 8 January 2025; accepted 17 January 2025. Date of publication 21 January 2025; date of current version 20 March 2025. This work was supported in part by the National Natural Science Foundation of China under Grant 52401406, in part by the Taishan Scholars of Shandong Province under Grant tsqnz20240801, and in part by the Major Scientific and Technological Innovation Project of Shandong Province of China under Grant 2022ZLGX04. Recommended for publication by Associate Editor J. Biela. *(Corresponding author: Chunwei Cai.)*

Chenghao Li, Xiuyun Ren, Xichen Liu, Shuai Wu, and Chunwei Cai are with the College of New Energy, Harbin Institute of Technology-Weihai, Weihai 264200, China, and also with the Key Laboratory of Cross-Domain Synergy and Comprehensive Support for Unmanned Marine Systems, Ministry of Industry and Information Technology, Weihai 264209, China (e-mail: 23b906007@stu.hit.edu.cn; renxiuyun@hit.edu.cn; 21s030155@stu.hit.edu.cn; wushuai@hit.edu.cn; caichunwei@hit.edu.cn).

Mingdong Qi is with State Grid Ningbo Electric Power Supply Company, Ningbo 310007, China (e-mail: 21s130569@stu.hit.edu.cn).

Jinpeng Yu is with the School of Automation, Qingdao University, Qingdao 266071, China (e-mail: yjp1109@qdu.edu.cn).

This article has supplementary material provided by the authors and color versions of one or more figures available at https://doi.org/10.1109/TPEL.2025.3532279.

Digital Object Identifier 10.1109/TPEL.2025.3532279

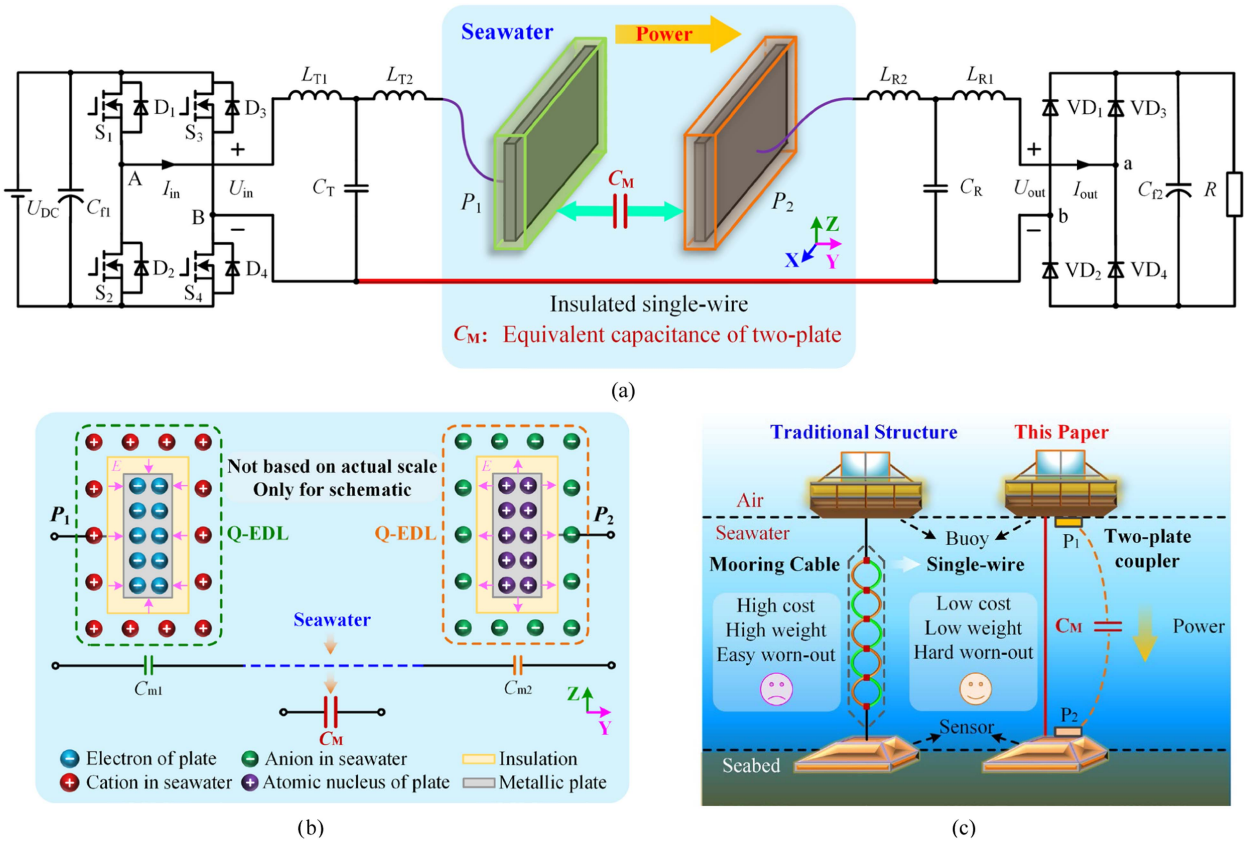

Fig. 1. General schematic of the proposed SCPT system. (a) Circuit diagrams. (b) Model of seawater electric-field coupled channel basing Q-EDL. (c) Comparison with traditional structure.

of seawater, seawater CPT is fundamentally different from pure water and fresh water. The most significant difference is that although seawater has a higher relative permittivity of 81 than air, the connection effect of seawater acting as a conductor is so much stronger than capacitive coupling that capacitive coupling can be ignored, which is a special property distinguished from traditional CPT. The bare electronic is firstly utilized in seawater capacitive power transfer (SCPT) [15], [16], [17]. Owing to electrolytic reaction, the power capacity can be only milliwatts which are not suitable for underwater sensor. To avoid direct contact between coupler and seawater, two seawater bags are placed between the transmitting and receiving plates in [18] and a mechanical damper is designed to separate the transmitting and receiving plates [19] and a dual-cavity separating two couplers of the same side program is proposed in [20]. The aim of these methods is all to cut off strong self-coupling path owing to the high conductivity of seawater. However, these methods are challenging to apply in practice. To eliminate the safety hazard to nearby organisms and equipment and shield from outside interference, a six-plate program which has four power transfer plates and two shielding plates is investigated in [21]. Based on this six-plate structure, a novel design approach employs different dielectric materials between the plates for underwater CPT is proposed in [22], where the coupling coefficient is enhanced, maintaining an efficiency over 80% with long distance and misalignment in freshwater, but feasibility or variation of model in seawater is not elaborated. It is important to notice that seawater is rich in a large number of ions, which is greatly different from freshwater. The model of four-plate insulated coupler with and without insulation layer in seawater is demonstrated [23]. However, the coupler is not completely submerged in seawater and the efficiency is 52.1% with only 6 mm distance. Drawing on the CPT with a single coupling capacitor in air, an underwater single-capacitor coupled WPT system with a 1m distance is proposed in [24]. One current pass is constituted by two plates and seawater, the other is realized by the connection of stray capacitance to ground in air. Besides, this method can also be utilized to transfer power and data to one or multiple loads simultaneously [25], [26] with maximum data rate up to 1MHz. Unfortunately, in actual ocean, the authors have found sea is connected to ground owing to high conductivity, which means seawater is involved in the coupling and no new connection between transmitter and receiver is established. The phenomenon of seawater connected to ground in actual ocean deserves to be noticed.

Considering conductivity of seawater and the connection to ground in actual ocean, a long distance, strong misalignment tolerance SCPT system with two insulated couplers and single-wire for underwater sensor is proposed in this article.

II. Overview of Proposed System

Fig. 1 is the general schematic of the proposed SCPT system. As shown in Fig. 1(a), one current pass is constituted by two

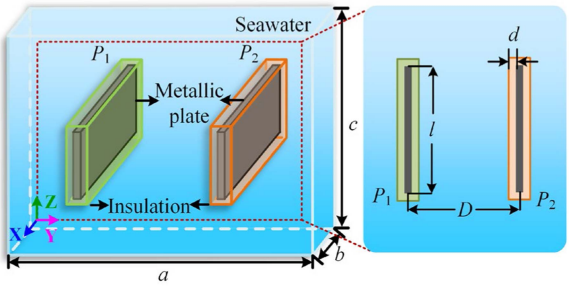

Fig. 2. Structure of the electric-field coupler. .

TABLE I
DIMENSIONS OF THE ELECTRIC-FIELD COUPLER IN SEAWATER

Parameter	Defined	Parameter	Defined
a	Water length	d_{12}	Plate distance
b	Water width	d	Insulation thickness
c	Water height	l	Plate length

insulated coupled plates and seawater, and the other is realized by the insulated single wire. Unlike air and freshwater, seawater has a conductivity of 4 S/m. To avoid the occurrence of electrolytic water reaction which leads to the loss of transmission power, an insulation layer covering the metallic plate is necessary shown in Fig. 2, and dimensions of the coupler is given in Table I.

As an important link in power transmission, performance of electric-field coupler is analyzed in detail basing quasi electric double layer (Q-EDL). For traditional EDL theory in electrochemistry, there should be a real exchange of charged particles between metallic plate and seawater. However, owing to the insulation layer, EDL is not entirely applicable to this article. Therefore, Q-EDL is more rigorous and precise. It can be demonstrated there is almost no potential drop in seawater, indicating that seawater between the coupled plates can be considered as an equipotential medium, which is a characteristic of conductor. Moreover, model of seawater electric-field coupled channel basing Q-EDL is built to guide the design of system, shown in Fig. 1(b). The feasibility of long-distance and strong-misalignment tolerance for couplers is verified by both theoretical analyses and experiments, which proves the corrections of Q-EDL analyze method and model of seawater electric-field coupled channel.

To enhance the ability of power transmission, a double *T-LCL* compensation network is investigated and selected. Constant output voltage, zero phase angle (ZPA), and antifrequency-offset are all obtained simultaneously, which demonstrates great potential for power supply of underwater sensor.

The program of this article is a trade-off between traditional mooring cable and wireless CPT with the advantages of low cost, low weight and hard worn-out shown in Fig. 1(c). In actual ocean test, the length of single-wire has reached 10 m with 206.8 W power transmission and 83% efficiency. The contributions of this article can be clarified as follows.

1) Based on Q-EDL theory, the law of potential drop in seawater near the coupler is clarified, and the feasibility of seawater as a conductor in SCPT is demonstrated from microscopic view.
2) Model of seawater electric-field coupled channel is proposed, and a double *T-LCL* compensation network is investigated, achieving constant output voltage, ZPA and antifrequency-offset simultaneously.
3) A single-wire SCPT scheme for underwater sensor is proposed. The results initially demonstrate the feasibility of proposed scheme in actual ocean and the advantages of long distance and strong misalignment.

TABLE II
MAIN PARAMETERS UTILIZED IN ANALYSES

Parameter	Defined
n_+	concentration of Na^+ ions (mol/m^3)
n_-	concentration of Cl^- ions (mol/m^3)
$n_{+\infty}$	stable concentration of Na^+ at infinity (mol/m^3)
$n_{-\infty}$	stable concentration of Cl^- at infinity (mol/m^3)
n_0	natural anion/cation concentrations in ocean (mol/m^3)
z_+	valence of Na^+ ions
z_-	valence of Cl^- ions
z_0	natural anion/cation valence in ocean
$\varphi(y)$	potential in y-direction
T	thermodynamic temperature (K)
e	electric charge of an electron (C)
k_B	Boltzmann constant (J/K)

III. ANALYSIS OF SEAWATER ELECTRIC-FIELD COUPLED CHANNEL

A. Microscopic Analysis of Electric-Field Coupler

Different from traditional medium of CPT, such as air and freshwater, seawater is rich in a large number of ions. When an excitation is applied to a metallic plate, the charge on the plate cannot flow into the seawater due to the presence of the insulation layer. When the metallic plate is negatively charged, anions in the ocean are repelled away and cations are attracted to the plate simultaneously, forming a layer of cations at the solid-liquid interface of the insulation layer and vice versa for positively charged. This is similar to the Q-EDL theory in electrochemistry. Thus, the microscopic transport mechanism in the electric-field coupled channel of seawater is investigated using the Gouy–Chapman–Stern model in electrochemistry. The main parameters utilized in analyze are given in Table II.

Assuming a simplified composition, seawater is considered to consist solely of Na^+ and Cl^- ions, with an ionic concentration of 500 mol/m^3, disregarding the presence of other free ions. To maintain electrical neutrality, it is assumed that the oceans have equal concentrations of anions and cations in their natural state. The relationships can be expressed as

$$\begin{cases} n_{+\infty} = n_{-\infty} = n_0 = 500 \text{ mol/m}^3 \\ z_+ = -z_- = z_0 = 1 \end{cases}. \tag{1}$$

The coupled plate has a front surface with a significantly larger area compared to sides, as shown in Fig. 2. Therefore, it can be considered the charge on the front side of the plate plays a dominant role in coupling device, while the charge on the sides is negligible. The diffusion of ions can be considered to occur in y-direction mainly. The charged insulated metal plate generates an electric field in its surroundings, which attracts ions from seawater to form an ionic layer at the interface between the solid and liquid. As the free ions are considered as plasmas, their diffusion in y-direction along the solid-liquid interface will follow the Boltzmann distribution

$$\begin{cases} n_+ = n_{+\infty} \mathrm{e}^{\frac{-z_+ e\varphi(y)}{k_B T}} = n_0 \mathrm{e}^{\frac{-z_0 e\varphi(y)}{k_B T}} \\ n_- = n_{-\infty} \mathrm{e}^{\frac{-z_- e\varphi(y)}{k_B T}} = n_0 \mathrm{e}^{\frac{z_0 e\varphi(y)}{k_B T}} \end{cases}. \tag{2}$$

The charge concentration ρ_e at a distance y from the solid-liquid interface is

$$\rho_e = \sum_{i=1}^{2} n_i z_i e = 2 z_0 e n_0 \sin h \left(\frac{z_0 e \varphi(y)}{k_B T} \right). \tag{3}$$

The charge concentration and potential magnitude at position y from the solid-liquid interface can be described by Poisson's equation. In order to focus on the change in potential, Boltzmann distribution is substituted into Poisson's equation only considering the y component, leading to the following Poisson–Boltzmann equation:

$$\frac{d^2\varphi(y)}{dy^2} = -\frac{\rho_e}{\varepsilon_0 \varepsilon_r} = \frac{2 z_0 e n_0}{\varepsilon_0 \varepsilon_r} \sin h \left(\frac{z_0 e \varphi(y)}{k_B T} \right). \tag{4}$$

Assuming the potential is zero at infinity, the potential is φ_0 at the solid-liquid interface, (4) is solved as

$$\varphi(y) = \frac{2 k_B T}{e z_0} \ln \left(\frac{1 + Z e^{-\sqrt{\frac{2 z_0^2 e^2 n_0}{\varepsilon_0 \varepsilon_r k_B T}} y}}{1 - Z e^{-\sqrt{\frac{2 z_0^2 e^2 n_0}{\varepsilon_0 \varepsilon_r k_B T}} y}} \right), Z = \frac{e^{\frac{e z_0 \varphi_0}{2 k_B T}} - 1}{e^{\frac{e z_0 \varphi_0}{2 k_B T}} + 1}. \tag{5}$$

According to the Debye–Huckel approximation method, (5) can be further simplified as

$$\varphi(y) = \varphi_0 \mathrm{e}^{-\sqrt{\frac{2 z_0^2 e^2 n_0}{\varepsilon_0 \varepsilon_r k_B T}} y} = \varphi_0 \mathrm{e}^{-ay}, e^{\frac{e z_0 \varphi_0}{k_B T}} = 1 + \frac{e z_0 \varphi_0}{k_B T} \tag{6}$$

which suggests that the potential in the solid-liquid interface region drops approximately following an exponential law.

Based on analysis above, a charged insulating metal plate in seawater can create a Q-EDL, shown in Fig. 3. The presence of this Q-EDL also establishes an electric field within the insulation. As a result, equivalent coupling capacitances C_{eq} are formed between metal plate and seawater. Within the solid-liquid interface region, potential drop follows an exponential law.

To further determine the geometric scale of potential drop, define the Debye length expression as

$$\lambda_D = \sqrt{\frac{\varepsilon_0 \varepsilon_r k_B T}{2 z_0^2 e^2 n_0}} \tag{7}$$

where refers to the distance over which the electric field can exert its influence on an individual charge within a plasma. According to (6) and (7), diffusion potential at the solid-liquid interface exhibits a rapid drop in y-direction. Within one λ_D as a scale, its value diminishes to approximately 0.3678 times the initial potential value at the solid-liquid interface. An electrochemical simulation model was developed to study the diffusion potential of the plate. The model utilizes seawater as the electrolyte solution, with Na^+ and Cl^- ions as the sole components, each having a concentration of 500 mol/m^3. At standard atmospheric pressure and a temperature of 25 °C, λ_D is determined to be approximately 0.437 nm.

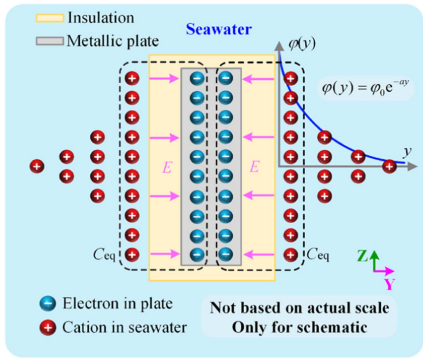

Fig. 3. Schematic diagram of Q-EDL for electric-field coupler in seawater.

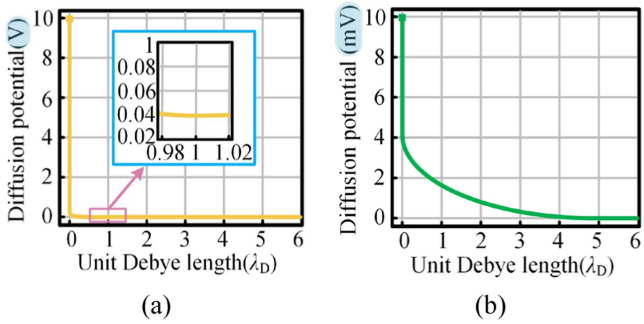

Fig. 4. Diffusion potential distribution at different excitation voltages. (a) 10 V. (b) 10 mV.

The diffusion potential distribution is depicted in Fig. 4. It is observed that irrespective of the initial potential value at the solid-liquid interface, whether it is high or low voltage, the diffusion potential diminishes significantly within one or several Debye lengths. Furthermore, beyond a few nanometers in the solution, the potential no longer exhibits a further decrease. Simultaneously, there is a significant abrupt decrease in potential at the solid-liquid interface compared to the potential at the surface of the plate. These results suggest that the majority of the potential drop takes place within the solid-liquid interface, while there is minimal voltage drop in seawater. Consequently, seawater can be considered as an equipotential medium.

A finite element simulation model of the two-plate coupling device in seawater is built in COMSOL to prove the analyze above. The material of the metallic plate and insulation are selected as aluminum and glass, respectively. The size of the metallic plate is 160 mm∗100 mm∗3 mm, and thickness of glass is 5 mm for better observation. The operating frequency of the system is set to be 300 kHz and simulation area is set as an

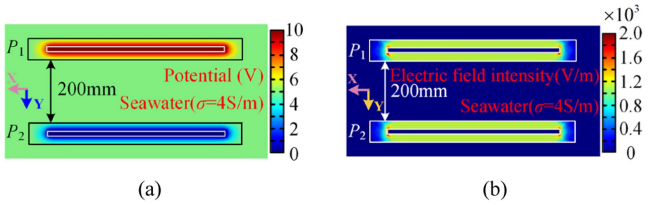

Fig. 5. Simulation results of two plates in seawater. (a) Potential (V). (b) Electric field intensity (V/m).

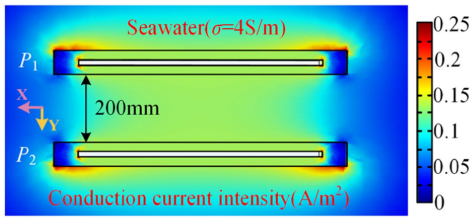

Fig. 6. Simulation result of current of two-plate in sea water.

infinite region. When the voltage of 10 V and 0 V are applied to P_1 and P_2 respectively, the simulation results are shown in Fig. 5. It can be observed that there is almost no potential drop in seawater, indicating that seawater between the coupled plates can be considered as an equipotential medium, and the majority of potential drop occurs in insulation.

B. Model of Seawater Electric-Field Coupled Channel

According to the Q-EDL and analysis of potential drop law based on the Debye length, potential drop in seawater mainly occurs at solid-liquid interface within a few nanometers.

The following assumptions can be made: When the coupling device is in an ac circuit, the continuously changing electric layers on both sides of the insulating material form an alternating electric field with continuously changing direction in the insulating medium. This manifests as a capacitive property related to the insulating medium rather than seawater. Considering the diffusion potential, it is important to note that the directional movement of free ions in seawater can be influenced. This movement is driven by electric field forces, resulting in the generation of current shown in Fig. 6. It is worth mentioning that this current exhibit resistive properties and consumes electrical energy in the process.

The capacitance value should satisfy the following conditions:

$$C = \frac{\varepsilon_0 \varepsilon_r S}{d} \tag{8}$$

where ε_r is the relative permittivity of insulation, S is the opposite area of Q-EDL, and d is the spacing between two layers.

In practice, the metallic plates covered with insulation in seawater can be regarded as a hexahedron. In theory, each face of this hexahedron has a capacitance formed by the quasi-electric double layer, and C_m is equivalent to the parallel combination of C_{up}, C_{down}, C_{front}, C_{back}, C_{left}, and C_{right}, as shown in Fig. 7.

Based on the above analysis, a seawater two-plate electric-field coupled channel conduction model can be proposed as

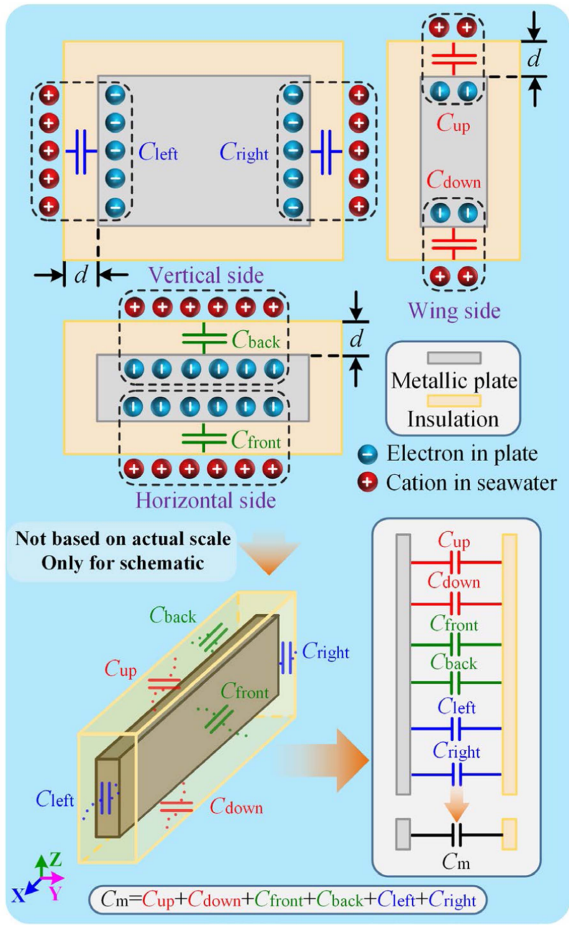

Fig. 7. Schematic diagram of equivalent capacitance of metallic plate covered with insulation in seawater.

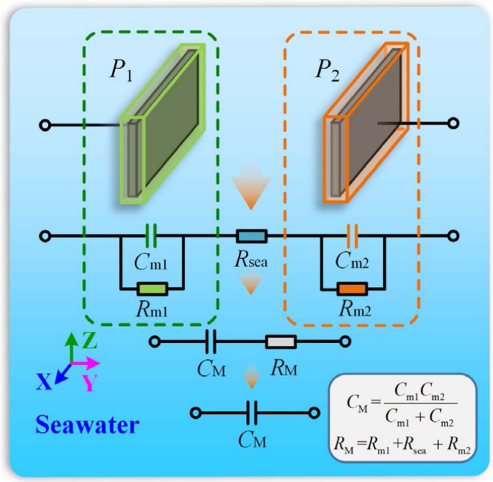

Fig. 8. Model of seawater electric-field coupled channel.

shown in Fig. 8, where C_{m1} and C_{m2} are the equivalent capacitances formed between the metallic plate and solid-liquid interface. C_M is equivalent to the series combination of C_{m1} and C_{m2}. R_{m1} and R_{m2} are the resistances of dielectric loss in insulation, and R_{sea} is the resistance of seawater. R_M is equivalent to the series combination of R_{m1}, R_{m2}, and R_{sea}.

TABLE III
THEORETICAL VALUES OF THE CAPACITANCES

Parameter	Value	Parameter	Value
C_{up}	0.03276nF	C_{right}	0.01048nF
C_{down}	0.03276nF	C_{m1}	10.56984nF
C_{front}	5.24168nF	C_{m2}	10.56984nF
C_{back}	5.24168nF	C_M	5.28492nF
C_{left}	0.01048nF	-	-

To simplify analysis, the influence of R_M is ignored in this article for its relatively small value, and further research will be conducted in the future. The material of the metallic plate and insulation are selected as aluminum and glass, respectively. The size of the metallic plate is 500 mm×160 mm×1 mm. The glass has a thickness of 1 mm, as indicated by d in Fig. 7, and the relative permittivity ε_r is 7.4.

According to (8), the theoretical values of the capacitance of six double layers formed by P_1 can be calculated. Due to the symmetry of the structure, P_2 has the same parameter values as P_1. Thus, C_{m1}, C_{m2}, and C_M can also be calculated, as given in Table III.

To demonstrate the rationality of the model, a finite-element simulation model is also built in COMSOL. The simulation value of C_{m1}, $C_{m2,}$ and C_M are 10.69049, 10.67253, and 5.34521 nF, respectively. The high agreement between the simulation values and the theoretical values demonstrates the rationality and feasibility of the model of seawater electric-field coupled channel proposed in Fig. 8.

According to the proposed Q-EDL theory, the equivalent capacitance C_M is formed by the series connection of the double-layer capacitance C_{m1} and C_{m2}. Notably, C_{m1} and C_{m2} are both formed by the metallic plate, insulation and seawater at the solid-liquid interface according to Q-EDL theory. It is the thickness d and relative permittivity ε_r of the insulation and the area of the metallic plate that affect C_{m1} and C_{m2}. Although seawater has a higher relative permittivity than air, it does almost no contribution to capacitive coupling but rather acts as conductor connection, which is consistent with the theoretical analysis in Section II-A. This is a special property different from air and fresh water completely. The internal resistance of the coupling device is mainly composed of the internal resistance of the seawater R_{sea} and the dielectric loss resistance R_{m1} and R_{m2}. To simplify the analysis, all the resistances of couplers are not considered.

When two coupled plates are misaligned or distance changes significantly, the relative positions of the metallic plates, insulation, and seawater near the solid-liquid interface remain unchanged. Therefore, the double-layer capacitances C_{m1} and C_{m2} do not change, and the equivalent capacitance C_M and the dielectric loss resistance R_{m1} and R_{m2} also remain unchanged. Due to the high conductivity of seawater, R_{sea} has a relatively small value.

Besides, though the simulation and experimental results, it can be found that when seawater fully wraps around two couplers, R_{sea} will initially increase with the increasement of transmission distance, however, it will eventually converge to an essentially stable value, which is different from traditional concept that R_{sea} is similar to the resistance of wire that will be always increasing with the increase of distance. In other words, when plates are completely submerged in seawater, the distance will influence R_{sea}, but the effect is limited. Thus, the coupling channel of the seawater electric-field theoretically possesses the feasibility of achieving long-distance and robust power transmission with strong-misalignment tolerance, which will be demonstrated as following.

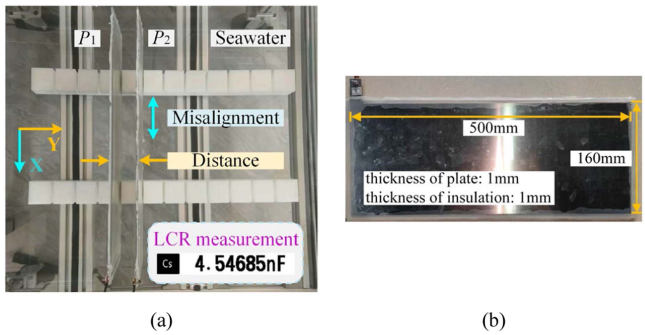

Fig. 9. Electric-field coupled plates. (a) Two-plate coupling device in seawater. (b) Dimensions of aluminum-glass plate.

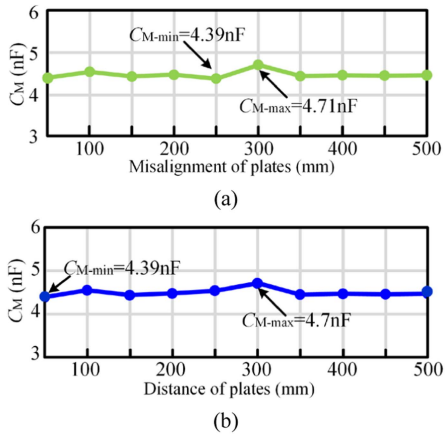

Fig. 10. C_M at different test condition. (a) Test result of misalignment. (b) Test result of distance variations.

C. Misalignment and Distance Variations Test

The structure of electric-field coupled plates is shown as Fig. 9. Each plate is made by sandwiching a 1mm-thick aluminum plate between two 1mm-thick glass plates. The value of C_M measured by LCR is 4.54685 nF. Considering the presence of air gap between the glass and aluminum plate, the actual measured value will be slightly smaller than the theoretical analysis value.

When the misalignment shifts from 50 mm to 500 mm, the average value of C_M is 4.523 nF, and the maximum value of C_M deviates from the average value by about 4.134%, as shown in Fig. 10(a). When the distance shifts from 50 to 500 mm, the average value of C_M is 4.505 nF, and the maximum value of C_M deviates from the average value by about 4.329%, as

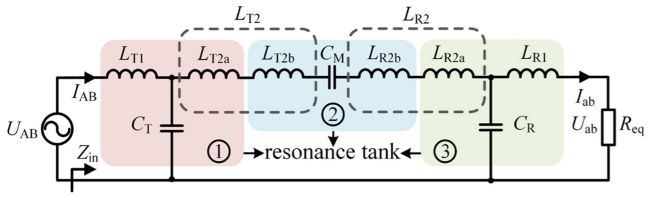

Fig. 11. Equivalent circuit of power channel.

shown in Fig. 10(b). The indicate that the coupling channel of the seawater electric-field does possess the feasibility of achieving long-distance and robust power transmission with strong-misalignment tolerance. This feature excels in adapting to intricate underwater environments and verifies the reasonableness of the proposed model of seawater electric-field coupled channel.

IV. Analysis and Design of Power Transfer Channel Based on Single-wire

A. Analysis and Design of Power Transfer Channel

The equivalent circuit of power channel is as shown in Fig. 11 and a double *T-LCL* compensation network is selected. L_{T2} and L_{R2} are further divided into L_{T2a}, L_{T2b} and L_{R2a}, L_{R2b}, respectively. There are three resonance tanks and the components of the resonance tank satisfy

$$\begin{cases} \omega_0^2(L_{T2b}+L_{R2b})C_M=1 \\ \omega_0^2 L_{T1}C_T=\omega_0^2 L_{T2a}C_T=1 \\ \omega_0^2 L_{R1}C_R=\omega_0^2 L_{R2a}C_R=1 \end{cases} \tag{9}$$

where ω_0 is the resonant angular frequency. The compensation elements affected by C_M are controlled to be within L_{T2} and L_{R2}, and the rest of parameters will not be affected by C_M, which reduces parameter sensitivity of the compensation network favorably.

The dc power supply U_{DC} is converted into ac voltage through the full-bridge inverter. U_{AB} is the root mean square value of the fundamental harmonic full-bridge output voltage and can be expressed as

$$U_{AB}=\frac{2\sqrt{2}}{\pi}U_{\mathrm{DC}}. \tag{10}$$

For the convenience of the subsequent study, the parameters are defined according to (11), where ω is the angular frequency, ω_n is the normalized angular frequency and Q is the quality factor

$$a=\frac{L_{T1}}{L_{R1}}, \omega_n=\frac{\omega}{\omega_0}, Q=\frac{\omega_0 L_{R1}}{R_{\mathrm{eq}}}, R_{\mathrm{eq}}=\frac{8}{\pi^2}R. \tag{11}$$

According to Fig. 11, the input impedance Z_{in} of the system at any angular frequency can be expressed as

$$Z_{\mathrm{in}}=\frac{X_{Z1}}{\frac{j\omega_n X_{Z1}}{\omega_0 L_{R1}a}+1}+j\omega_0\omega_n L_{R1}a \tag{12}$$

where

$$\begin{cases} X_{Z1}=\frac{j\omega_n}{2\omega_0 C_M}+j\omega_0\omega_n L_{R1}a+ \\ \left(\left(\frac{X_{Z2}}{\frac{j\omega_n X_{Z2}}{\omega_0 L_{R1}}+1}+\frac{j\omega_n}{2\omega_0 C_M}+j\omega_0\omega_n L_{R1}\right)\right. \\ \left.\times j\omega_0\omega_n C_M+1\right)/(j\omega_0\omega_n C_M) \\ X_{Z2}=j\omega_0\omega_n L_{R1}+\frac{\omega_0 L_{R1}}{Q} \end{cases}. \tag{13}$$

Moreover, based on the nodal voltage equation, the output voltage U_{ab} of the system at any angular frequency can be expressed as

$$U_{ab}=\frac{\omega_0 L_{R1}}{QX_{G1}X_{G3}(\frac{X_{G2}}{X_{G1}}+j\omega_0\omega_n L_{R1}a)}\cdot U_{AB}. \tag{14}$$

Working at resonant angular frequency ω_0, the input impedance Z_{in} and the output voltage U_{ab} of the system can be expressed as (16). According to (16), ZPA can be obtained when the system working at resonant angular frequency ω_0 and furthermore, a constant output voltage can also be realized based on constant input voltage

$$\begin{cases} X_{G1}=\frac{j\omega_n X_{G2}}{\omega_0 L_{R1}a}+1 \\ X_{G2}=\frac{j\omega_n}{2\omega_0 C_M}+j\omega_0\omega_n L_{R1}a-j\cdot\left(j\omega_0\omega_n C_M\right. \\ \left.\times\left(\frac{j\omega_0\omega_n L_{R1}+\frac{\omega_0 L_{R1}}{Q}}{X_{G3}}+\frac{j\omega_n}{2\omega_0 C_M}+j\omega_0\omega_n L_{R1}\right)+1\right)/\omega_0\omega_n C_M \\ X_{G3}=\frac{j\omega_n(j\omega_0\omega_n L_{R1}+\frac{\omega_0 L_{R1}}{Q})}{\omega_0 L_{R1}}+1 \end{cases} \tag{15}$$

$$\begin{cases} Z_{\mathrm{in}}=\frac{a^2\omega_0 L_{R1}}{Q} \\ U_{ab}=-\frac{1}{a}\cdot U_{AB}=-\frac{L_{R1}}{L_{T1}}\cdot U_{AB} \end{cases}. \tag{16}$$

The electric-field coupled devices of the system have been identified. According to the measurement results, C_M takes the value of 4.5 nF, the resonant frequency f_0 is selected to be 300 kHz, and L_{T2b} and L_{R2b} can be calculated as 31.272 μH, respectively, based on (9). Considering of the volume and weight of the compensation inductor, C_T and C_R are both selected to be 15 nF, L_{T1} and L_{T2a} is initially determined to be 18.7632 μH, and a is selected as 1 where a symmetric construction can be obtained for a simpler and clearer design.

Generally, the system compensation parameters are designed for the resonance case, so it is usually expected that the system always operates at the resonance frequency. However, during the operation of the system, certain fault conditions are always encountered that make the operating frequency of the system deviate from its intrinsic resonant frequency, especially in complex environment of seawater. Since Q varies with load, it is necessary to study not only the frequency characteristics of the input impedance phase when Q is fixed, but also the relationship between the input impedance phase α_z and Q when the frequency is fixed, i.e., the stability of the ZPA state when the load varies.

Fig. 12 shows the α_z-ω_n curve chart under different Q values, where ω_n represents the normalized frequency. When $Q=1.6$, the curve can almost maintain ZPA state smoothly and stably as ω_n is between 0.7 and 1. When Q takes other values, the curve near ZPA state point has a significant rate of change and a small frequency offset may cause a large phase change

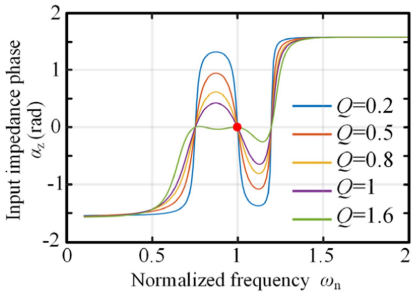

Fig. 12. α_z-ω_n curves at different Q ($L_{R1} = 18.7632\ \mu$H, $a = 1$).

TABLE IV
PARAMETERS OF POWER TRANSFER COMPENSATION NETWORK

Parameter	Value	Parameter	Value
C_T	15nF	C_R	15nF
L_{T1}	18.7632μH	L_{R1}	18.7632μH
L_{T2a}	18.7632μH	L_{R2a}	18.7632μH
L_{T2b}	31.272μH	L_{R2b}	31.272μH
C_M	4.5nF	Q	1.6
f_0	300kHz	ω_n	1

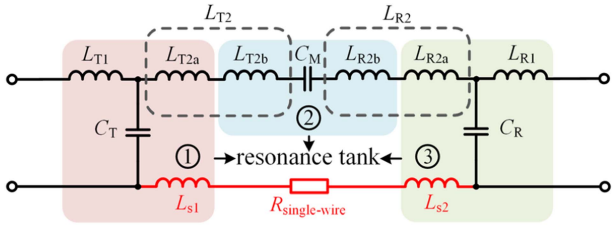

Fig. 13. Resonant tank considering the parasitic inductance and resistance of single-wire.

of Z_{in}. In addition, the change rate of α_z is obviously greater when ω_n decreases from 0.753, compared with increasing from 1. The system working point is preliminarily selected as the red point, for $Q = 1.6$, $\omega_n = 1$. The parameters of double *T-LCL* compensation have been selected and verified, as given in Table IV.

B. Impact of Single-Wire

When the single-wire is short, the parasitic inductance L_s of it is small and can be ignored. Nevertheless, when the single-wire is long, the parasitic inductance L_s should be considered [11]. The resonant tank considering the parasitic inductance of single-wire is shown in Fig. 13. The parasitic inductance L_s is equated to the series connections of two inductors L_{s1} and L_{s2}. The components of the modified resonance tank satisfy (17). Compared with the case where the parasitic inductance L_s of the single-wire is not considered shown as (9), the only affected parameters are L_{T2a} and L_{R2a}. This indicates that, by simply adjusting L_{T2a} and L_{R2a} with respect to the parasitic inductance of single-wire, the ideal resonance can still be maintained, without affecting other properties. Besides, the parasitic resistance of single-wire $R_{\text{single-wire}}$ will rise with increasing transmission distance, affecting the system efficiency, which must be emphasized in future studies

$$\begin{cases} \omega_0^2(L_{T2b} + L_{R2b})C_M = 1 \\ \omega_0^2 L_{T1}C_T = \omega_0^2(L_{T2a} + L_{s1})C_T = 1 \\ \omega_0^2 L_{R1}C_R = \omega_0^2(L_{R2a} + L_{s2})C_R = 1 \end{cases}. \tag{17}$$

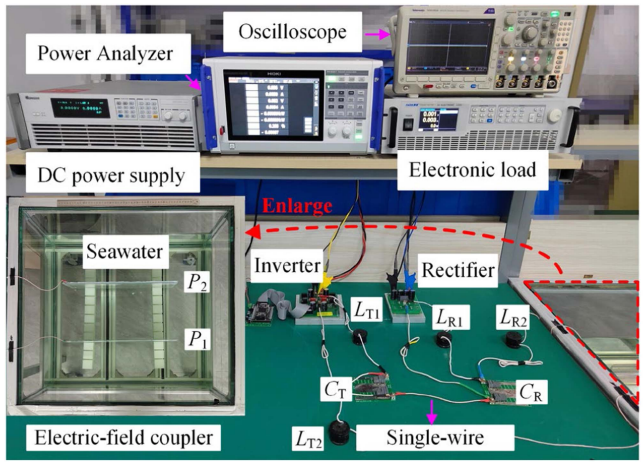

Fig. 14. Test bench of experimental verification in lab.

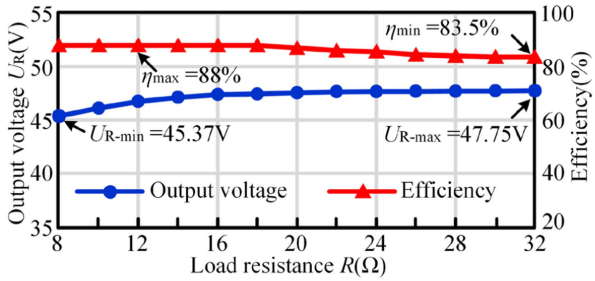

Fig. 15. 300 kHz–50 V Constant output voltage test results.

V. EXPERIMENTAL VERIFICATION

A. Experiment in Lab

A two-plate SCPT prototype is built in lab, as shown in Fig. 14. Owing to the length of single-wire is short, the parasitic inductance can be ignored and the resonance condition follows (9). The main parameters are selected based on Table IV. The system is powered by dc source U_{DC} and a general inverter containing four SiC MOSFETs (IMZA65R027M1H) S_1-S_4 with 35 mΩ drain-source on-state resistance is used to supply high frequency alternating excitation for compensated circuit. At output side, the four diodes $D_1 - D_4$ forms a rectifier to convert ac to dc for the load resistance R_L. P_1 and P_2 are all submerged in seawater. To ensure the authenticity of the experiment, real seawater salvaged from the ocean is applied rather than salt water prepared in lab.

When the driving dc voltage U_{DC} is 50 V, the constant output voltage ability of the system is tested. The measured results are shown in Fig. 15, in which the output voltage and efficiency are both investigated when load resistance shifts from 8 to 32 Ω. It is shown that the two-plate SCPT system possesses the capability of constant output voltage and the efficiency obtained maximum value 88% when load resistance is 12 Ω.

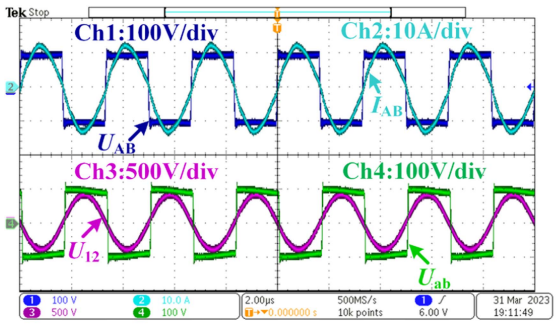

(a)

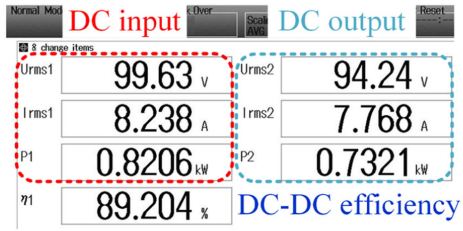

(b)

Fig. 16. 100 V–12 Ω Power transmission tests. (a) Waveforms of inverter output voltage U_{AB}, inverter output current I_{AB}, voltage across two-plate U_{12} and rectifier input voltage U_{ab}. (b) Power and efficiency test.

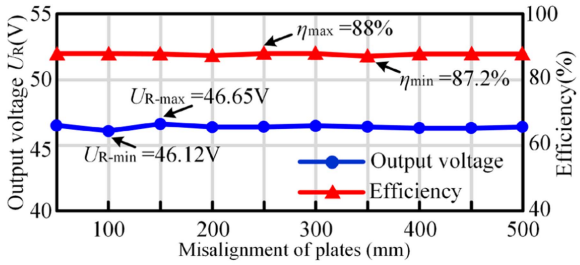

(a)

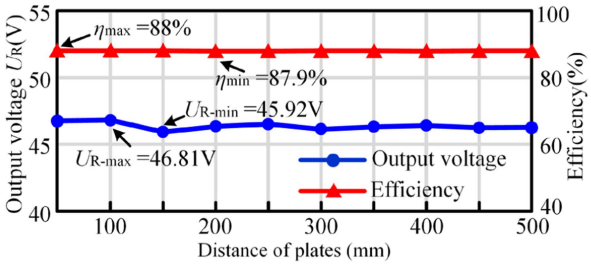

(b)

Fig. 17. 50 V-12 Ω Power transmission tests. (a) Misalignment test. (b) Distance variations test.

The measured system waveforms when dc voltage U_{DC} is 100 V and load resistance is 12 Ω are shown in Fig. 16, in which the output voltage U_{AB} and output current I_{AB} of inverter are basically in phase, ensuring the high efficiency operation of the inverters. The phase of input voltage U_{ab} of rectifier and U_{AB} are in opposite phase, which is consistent with theoretical derivation (16). The voltage U_{12} across two-plate is up to nearly 500 V with compensation network. The system transfers 732.1W of

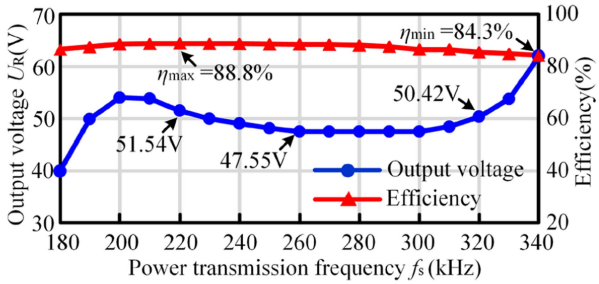

Fig. 18. 50 V-Q = 1.6 Frequency offset test results.

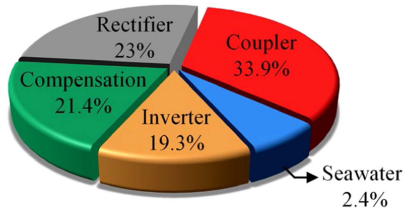

Fig. 19. Power loss distribution of the experiment in lab.

TABLE V
PARAMETERS OF POWER TRANSFER COMPENSATION NETWORK IN ACTUAL OCEAN

Parameter	Value	Parameter	Value
C_T	15nF	C_R	15nF
C_{m1}	16.4nF	C_{m2}	15.5nF
C_M	8nF	-	-
L_{T1}	18.7632μH	L_{R1}	18.7632μH
L_{T2a}	11.7632μH	L_{R2a}	11.7632μH
L_{T2b}	17.5μH	L_{R2b}	17.5μH
L_s	14uH	$L_{s1,2}$	7uH
f_0	300kHz	$R_{single\text{-}wire}$	2.6Ω

energy with 89.2% efficiency, promising a good energy transfer capability.

The experimental results are shown in Fig. 17 when the misalignment and distance variations separately occur. Load resistance is 12 Ω. It can be pointed that whatever output power or efficiency keeps stable when relative location varies, achieving stable power transfer.

The experimental results are shown in Fig. 18 when the frequency offset occurs. When the frequency fluctuation ranges from 220 to 320 kHz, the output voltage U_R has good resistance to frequency offset, which is consistent with the theoretical analysis shown in Fig. 12. This indicates the system has the frequency stability in voltage gain at a quality factor Q of 1.6. Besides, when a frequency offset occurs in the system, the transmission efficiency consistently remains above 84%, irrespective of any changes in the system voltage gain.

The power loss distribution of proposed two-plate SCPT system in lab measured experimentally is obtained in Fig. 19. Considering that the couplers and compensations are handmade, defects in manufacturing process causes increased losses to some extent. Besides, power loss in seawater is only 2.4%, which

TABLE VI
COMPARISON WITH EXISTING RESEARCH OF SEAWATER CAPACITIVE POWER TRANSFER

Reference	[18]	[19]	[20]	[23]	[25]	[26]	This article
Output power	100W	1kW	130W	15W	300W	1kW	732W
Resonant frequency	625kHz	6.78MHz	1.1MHz	210kHz	200kHz	200kHz	300kHz
Efficiency	80.15%	94.5%	81.2%	52.1%	91.07%	76%	89.2%
Means of implementation	Seawater bag	Partition damper	Dual-cavity	Seawater only between plates	Virtual path	Virtual path	Single-wire
Distance	150mm	20mm	300mm	6mm	1m	1m	500mm

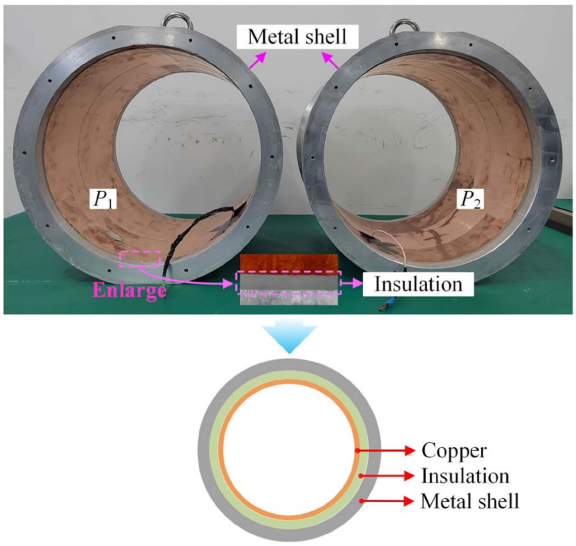

Fig. 20. Internal structure of sealed metal shell.

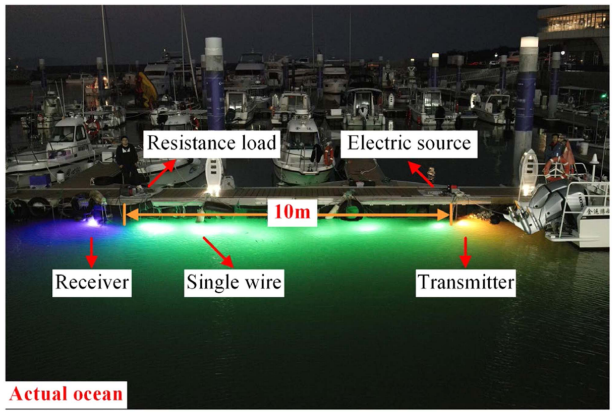

Fig. 21. Prototype of the two-plate SCPT system with 10m single-wire in actual ocean.

indicates that the coupling channel of the seawater electric-field possesses the feasibility of achieving long-distance power transmission. Although seawater can be considered as a conductor based above analysis, it does have resistance and it will be researched in depth later.

B. Experiment in Actual Ocean

To verify the feasibility of the proposed SCPT system for power transfer in actual ocean furtherly, two new seawater capacitive couplers with sealed metal shell are designed and an experiment in actual ocean is conducted.

The internal structure of sealed metal shell is shown as Fig. 20. The material of metal shell is aluminum. As insulation, a silicone pad is covered inside the metal shell. Then, the copper foils used as metal plate are attached to the silicone pad to form the coupler. Copper, insulation and metal shell form an equivalent capacitance. Besides, the metal shell is sealed with two metal covers. One cover is used for waterproof connection with dc input, output and single-wire. The other cover is used for circuit elements, which are fixed in the metal cover utilizing the acrylic stent to protect the components from connecting the metal shell.

Then, the circuit elements including inverter, compensation and rectifier are all sealed in metal shell. A two-plate CPT experiment with 10m single-wire in actual ocean is conducted, as shown in Fig. 21. The geographic location of the experimental area is (122° 06′ 26.1″E, 37° 32′ 45.3″N). Considering the parasitic inductance of single-wire L_s, main parameters of experiment in actual ocean are selected based on Table V. To better display the single-wire completely immersed in seawater, a green LED strip is bundled on the single-wire. Both the transmitter and receiver are submerged in seawater illuminated with yellow and blue LEDs. All the circuit connections are waterproofed by watertight connectors. A 50 Ω resistor serves as the load and a multimeter is utilized to measure output voltage. Therefore, the key metrics of system such as efficiency, power, can be calculated. When the input voltage is 100 V, the experiment results achieve 206.8 W power transmission and 83% efficiency. Compared with the results in lab, there is an approximately 6% reduction in efficiency and the reason can might be attributed to the parasitic resistance of the single-wire and the seawater environment. Nevertheless, the experimental results have demonstrated the feasibility of the proposed scheme in actual ocean. In the future, methods to improve efficiency and distance will be researched.

According to above analysis, comparison of this article with existing research of SCPT is given in Table VI. Comparing the output power, efficiency and transfer distance, the scheme proposed in this article has a relatively good performance, especially the advantages of long distance.

VI. CONCLUSION

This article proposes a long-distance, strong-misalignment tolerance SCPT system with two insulated couplers and single-wire for underwater sensor. It is a tradeoff between traditional mooring cable with two strands of conductor wire and wireless CPT, possessing the characteristics of low cost, low weight and

hard worn-out. First, for insulated couplers in seawater, a Q-EDL theory is proposed and seawater between two couplers can be considered as equipotential medium is verified in detail. Then, a novel model of seawater electric-field coupled channel is built and the feasibility of long distance and strong misalignment tolerance for couplers is proved. Moreover, a double *T-LCL* compensation network is investigated and selected for constant output voltage, ZPA and antifrequency-offset. Experimental results in lab show that the system can deliver 732.1 W at a dc–dc efficiency of 89.2%. In actual ocean, the experimental transmission distance is 10 m, achieving 206.8 W power transmission and 83% efficiency, which verifies the proposed program is adapted to power supply of sensors in complex ocean environment and the advantages of long distance.

REFERENCES

[1] M. Chaudhary, N. Goyal, A. Benslimane, L. K. Awasthi, A. Alwadain, and A. Singh, "Underwater wireless sensor networks: Enabling, technologies for node deployment and data collection challenges," *IEEE Internet Things J.*, vol. 10, no. 4, pp. 3500–3524, Feb. 2023.

[2] R. Wang, R. Ma, Y. Zhang, G. Liu, and W. Kang, "An energy-efficient multimode transmission scheme for underwater sensor network," *IEEE Internet Things J.*, vol. 10, no. 22, pp. 19640–19654, Nov. 2023.

[3] C. Fang, X. Li, Z. Xie, J. Xu, and L. Xiao, "Design and optimization of an inductively coupled power transfer system for the underwater sensors of ocean buoys," *Energies.*, vol. 10, no. 1, pp. 84–102, Jan. 2017.

[4] S. Zhang, W. Yang, Y. Xin, R. Wang, and C. Li, "Research progress of a mooring buoy system for sea surface and seafloor observation," *Chin. Sci. Bull.*, vol. 64, no. 28, pp. 2963–2973, Oct. 2019.

[5] J. Yu, S. Zhang, W. Yang, and H. Gao, "Design and application of buoy single point mooring system with electro-optical-mechanical cable," *J. Mar. Sci. Eng.*, vol. 8, no. 9, pp. 672–697, Sep. 2020.

[6] C. Cai et al., "A resident subsea docking system with a real-time communication buoy moored by an electro-optical-mechanical cable," *Ocean Eng.*, vol. 271, pp. 113729–113744, Feb. 2023.

[7] S. Wu, C. Cai, L. Jiang, J. Li, and S. Yang, "Unmanned aerial vehicle wireless charging system with orthogonal magnetic structure and position correction aid device," *IEEE Trans. Power Electron.*, vol. 36, no. 7, pp. 7564–7575, Jul. 2021.

[8] J. Mai, Y. Wang, X. Zeng, Y. Yao, K. Wu, and D. Xu, "A multi-segment compensation method for improving power density of long-distance IPT system," *IEEE Trans. Ind. Electron.*, vol. 69, no. 12, pp. 12795–12806, Dec. 2022.

[9] C. Fang, X. Li, Z. Xie, J. Xu, and L. Xiao, "Design and optimization of an inductively coupled power transfer system for the underwater sensors of ocean buoys," *Energies*, vol. 10, no. 1, pp. 84–102, Jan. 2017.

[10] X. Cui, J. Xu, S. Pang, X. Li, and H. Li, "Design and implementation of inductively coupled power and data transmission for buoy systems," *Energies*, vol. 16, no. 11, pp. 4417–4436, May 2023.

[11] J. Xu, S. Pang, S. Pan, Q. Ma, X. Li, and H. Li, "Modeling and construction of underwater single-wire power transfer system," *IEEE Trans. Ind. Electron.*, vol. 71, no. 12, pp. 16792–16802, Dec. 2024.

[12] J. Xu, X. Li, Z. Xie, C. Fu, and R. Du, "Design and analysis of inductively coupled power transfer system on mooring buoy with double ultracapacitor chargers using indirect control," *IEEE Trans. Ind. Electron.*, vol. 67, no. 6, pp. 4836–4845, Jun. 2020.

[13] J. Xu, X. Li, H. Li, Z. Xie, and Q. Ma, "Maximum efficiency tracking for multitransmitter multireceiver wireless power transfer system on the submerged buoy," *IEEE Trans. Ind. Electron.*, vol. 69, no. 2, pp. 1909–1919, Feb. 2022.

[14] W. Zhou, D. Tang, Z. Chen, R. Mai, and Z. He, "Nonisolation model and load virtual-grounding design method for capacitive power transfer system with asymmetric four-plate coupling interface," *IEEE J. Emerg. Sel. Topics Power Electron.*, vol. 12, no. 1, pp. 208–218, Feb. 2024.

[15] M. Tamura, K. Murai, and D. Fujii, "Lightweight and high-efficiency coupler suitable for underwater WPT system," in *Proc. IEEE Asia-Pac. Microw. Conf.*, 2019, pp. 7–9.

[16] M. Tamura, K. Murai, and Y. Naka, "Capacitive coupler utilizing electric double layer for wireless power transfer under seawater," in *Proc. IEEE MTT-S Int. Microw. Symp.*, 2019, pp. 1415–1418.

[17] K. Murai and M. Tamura, "Improvements of transfer efficiency in capacitive wireless power transfer under seawater," in *Proc. IEEE Asia-Pac. Microw. Conf.*, 2019, pp. 714–716.

[18] L. Yang, M. Ju, and B. Zhang, "Bidirectional undersea capacitive wireless power transfer system," *IEEE Access*, vol. 7, pp. 121046–121054, Sep. 2019.

[19] M. Tamura, K. Murai, and M. Matsumoto, "Design of conductive coupler for underwater wireless power and data transfer," *IEEE Trans. Microw. Theory Techn.*, vol. 69, no. 1, pp. 1161–1175, Jan. 2021.

[20] H. Mahdi, B. Hoff, P. G. Ellingsen, and T. Østrem, "Conformal transformation analysis of capacitive wireless charging," *IEEE Access*, vol. 10, pp. 105621–105630, 2022.

[21] E. Rong, P. Sun, X. Zhang, G. Yang, and X. Wu, "3.3 kW Underwater capacitive power transfer system for electric ship charging application," in *Proc. IEEE Int. Conf. Power Sci. Technol.*, 2023, pp. 1052–1057, doi: 10.1109/ICPST56889.2023.10164993.

[22] E. Rong, P. Sun, K. Qiao, X. Zhang, G. Yang, and X. Wu, "Six-plate and hybrid-dielectric capacitive coupler for underwater wireless power transfer," *IEEE Trans. Power Electron.*, vol. 39, no. 2, pp. 2867–2881, Feb. 2024.

[23] C. Li, X. Qu, F. Kong, and C. Ma, "Modeling and characteristic analysis of four-plate coupler for underwater capacitive power transfer system," *Proc. CSEE*, doi: 10.13334/j.0258-8013.pcsee.232683.

[24] M. Nie et al., "A 1 kw, 76% efficiency underwater single-capacitor coupled WPT system with a 1 m separation distance single-capacitor coupled," *Int. J. Circuit Theory Appl.*, 2024, doi: 10.1002/cta.4221.

[25] C. Da, F. Li, L. Wang, C. Tao, S. Li, and M. Nie, "Analysis and implementation of underwater single capacitive coupled simultaneous wireless power and bidirectional data transfer system," *IEEE Trans. Ind. Electron.*, vol. 71, no. 12, pp. 15674–15684, Dec. 2024.

[26] C. Da, F. Li, M. Nie, S. Li, C. Tao, and L. Wang, "Undersea capacitive coupled simultaneous wireless power and data transfer for multi-load applications," *IEEE Trans. Power Electron.*, vol. 40, no. 1, pp. 2630–2642, Jan. 2025, doi: 10.1109/TPEL.2024.3483956.

Chenghao Li (Student Member, IEEE) was born in Liaoning Province, China, in 2000. He received the B.S. degree in electrical engineering, in 2023, from Harbin Institute of Technology, Weihai, China, where he is currently working toward the Ph.D. degree in electrical engineering.

His current research interests include long-distance seawater capacitive power transfer, mechanism of electromagnetic field and simultaneous wireless power and data transfer.

Xiuyun Ren (Member, IEEE) received the B.A. degree in physics and the M.S. degree in optics from Shandong Normal University, Jinan, China, in 2002 and 2005, respectively, and the Ph.D. degree in physical electronics from the Harbin Institute of Technology, Harbin, China, in 2016.

Since 2014, she has been an Associate Professor with the School of Information Science and Engineering, Harbin Institute of Technology at Weihai, Weihai, China. Her research interests include Lidar ocean exploration, wireless communication technology, and optoelectronic technology and their applications.

Xichen Liu (Student Member, IEEE) was born in Shandong Province, China, in 1998. He received the B.S. and M.S. degrees in electrical engineering in 2020 and 2023, respectively, from Harbin Institute of Technology, Weihai, China, where he is currently working toward the Ph.D. degree in electrical engineering.

His current research interests include power electronics and wireless power transfer system for autonomous underwater vehicles and unmanned aerial vehicles.

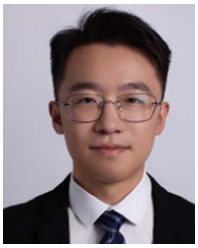

Shuai Wu (Member, IEEE) was born in Shanxi Province, China, in 1995. He received the B.S. degree in electrical engineering and automation from Shanxi Agricultural University, Jinzhong, China, in 2017, and the M.S. and Ph.D. degrees in electrical engineering from the Harbin Institute of Technology (HIT), Harbin, China, in 2019 and 2023, respectively.

Since 2023, he has been an Associate Professor with the School of New Energy, HIT at Weihai, China. His current research interests include wireless power transfer for unmanned vehicles and implanted biomedical devices.

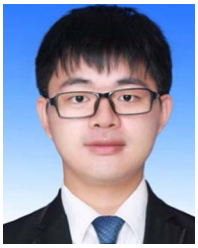

Mingdong Qi received the B.S. and M.S. degrees in electrical engineering and automation from Harbin Institute of Technology, Weihai, China, in 2021 and 2023, respectively.

He is currently with the State Grid Ningbo Electric Power Supply Company, Ningbo, China. His current research interests include wireless power transfer and inverters.

Jinpeng Yu (Senior Member, IEEE) received the B.Sc. degree in automation of Qingdao University, Qingdao, China, in 2002, the M.Sc. degree in system engineering of Shandong University, Jinan, China, in 2006 and the Ph.D. degree in system theory from the Institute of Complexity Science, Qingdao University, Qingdao, China, in 2011.

He is currently a Distinguished Professor at the School of Automation, Qingdao University, China. His research interests include electrical energy conversion and motor control, applied nonlinear control and intelligent systems.

Dr. Yu is a recipient of the Shandong Province Taishan Scholar Special Project Fund and Shandong Province Fund for Outstanding Young Scholars. He was an Associate Editor of several journals, including IEEE TRANSACTIONS ON CYBERNETICS, IEEE TRANSACTIONS ON NEURAL NETWORKS AND LEARNING SYSTEMS, IEEE TRANSACTIONS ON CIRCUITS AND SYSTEMS—PART I: REGULAR PAPERS, IEEE TRANSACTIONS ON CIRCUITS AND SYSTEMS—PART II: EXPRESS BRIEFS, *Information Sciences, Journal of The Franklin Institute, ISA Transactions, Journal of System Science and Complexity*, etc.

Chunwei Cai (Member, IEEE) was born in Shandong Province, China, in 1977. He received the B.S. and M.S. degrees in control theory and control engineering from Shan Dong University, Jinan, China, in 2001 and 2004, respectively; and the Ph.D. degree in electrical engineering from Harbin Institute of Technology (HIT), Harbin, China, in 2013.

Since 2006, he has been a Lecturer with HIT, Weihai, China. Since 2014, he has been a Professor with HIT at Weihai. His current research interests include wireless power transfer systems, power converters,